

01 Jan 1995

Methsnotrophic Biodegradation of Trichloroethylene in a Hollow Fiber Membrane Bioreactor

Carol E. Aziz

Mark W. Fitch


Missouri University of Science and Technology, mfitch@mst.edu

Larry K. Linqvist

Jonathan G. Pressman

et. al. For a complete list of authors, see https://scholarsmine.mst.edu/civarc_enveng_facwork/2421

Follow this and additional works at: https://scholarsmine.mst.edu/civarc_enveng_facwork

 Part of the [Architectural Engineering Commons](#), and the [Civil and Environmental Engineering Commons](#)

Recommended Citation

C. E. Aziz et al., "Methsnotrophic Biodegradation of Trichloroethylene in a Hollow Fiber Membrane Bioreactor," *Environmental Science and Technology*, vol. 29, no. 10, pp. 2574 - 2583, American Chemical Society, Jan 1995.

The definitive version is available at <https://doi.org/10.1021/es00010a018>

This Article - Journal is brought to you for free and open access by Scholars' Mine. It has been accepted for inclusion in Civil, Architectural and Environmental Engineering Faculty Research & Creative Works by an authorized administrator of Scholars' Mine. This work is protected by U. S. Copyright Law. Unauthorized use including reproduction for redistribution requires the permission of the copyright holder. For more information, please contact scholarsmine@mst.edu.

Methanotrophic Biodegradation of Trichloroethylene in a Hollow Fiber Membrane Bioreactor

CAROL E. AZIZ,[†] MARK W. FITCH,[‡]
LARRY K. LINQUIST,[†]
JONATHAN G. PRESSMAN,[†]
GEORGE GEORGIOU,[‡] AND
GERALD E. SPEITEL JR.*[†]

Department of Civil Engineering and Department of Chemical Engineering, University of Texas at Austin, Austin, Texas 78712

Biodegradation of trichloroethylene (TCE) in a hollow fiber membrane bioreactor was investigated using a mutant of the methanotrophic bacteria, *Methylosinus trichosporium* OB3b. Contaminated water flowed through the lumen (i.e., fiber interior), and the bacteria circulated through the shell side of the membrane module and an external growth reactor. In mass transfer studies with a radial cross-flow membrane module, 78.3–99.9% of the TCE was removed from the lumen at hydraulic residence times of 3–15 min in the lumen and the shell. In biodegradation experiments, 80–95% of the TCE was removed from the lumen at hydraulic residence times of 5–9 min in the lumen. The TCE transferred to the shell was rapidly biodegraded, with rate constants ranging from 0.16 to 0.9 L (mg of TSS)⁻¹ day⁻¹. Radiochemical data showed that over 75% of the transferred TCE was biodegraded in the shell, with the byproducts being approximately equally divided between carbon dioxide and nonvolatiles. This study shows that a hollow fiber membrane bioreactor system coupled with the mutant strain PP358 of *M. trichosporium* OB3b is a very promising technology for chlorinated solvent biodegradation.

Introduction

Contamination of groundwater and soils with chlorinated aliphatic solvents is a widespread problem in this country and in many other industrialized nations. Chlorinated aliphatic solvents, such as trichloroethylene (TCE), are of concern because of their toxicity and high frequency of occurrence. TCE is the most prevalent compound, having been found, for example, at 246 out of 1035 Superfund sites (1). A variety of biological treatment technologies for the destruction of chlorinated solvents are now under development. A large subset of these technologies is based on

pure or mixed cultures of aerobic bacteria that cometabolize chlorinated solvents.

In considering aerobic cometabolism of chlorinated solvents, classification of contamination problems into one of three categories is useful. The first category is contamination consisting of only chlorinated ethenes. These chemicals are easiest to address because their structure is similar, and a number of bacterial species can cometabolize them. Examples include bacteria growing on methane (methanotrophs) or simple aromatic chemicals, such as phenol and toluene. The aromatic degraders, in particular, are easy to grow and are relatively hardy organisms. The second category consists of contamination by one or more chlorinated methanes or ethanes, perhaps together with chlorinated ethenes. This second category of contamination is delineated because the range of available bacteria narrows. Aromatic degraders can only cometabolize chlorinated ethenes; therefore, methanotrophs have been investigated most widely when chlorinated methanes or ethanes must be treated. The third category of contamination, and one encountered frequently in practice, consists of mixed wastes in which chlorinated solvents are present in mixtures with other organic or inorganic chemicals. The main concern is the impact of the other chemicals on the cometabolism of chlorinated solvents. Inorganics, such as heavy metals, may be toxic to the bacteria, while organics may likewise be toxic and also may compete for the enzymes catalyzing the cometabolism, thereby slowing down reaction kinetics.

This research focused on identifying and demonstrating at the laboratory scale a technology that would be applicable to the second and third categories of chlorinated solvent contamination. Therefore, a methanotroph was selected to provide the potential for degrading a broad range of chlorinated solvents. Many pure and mixed cultures of methanotrophs can cometabolize chlorinated solvents, but among the best known rates are those attributed to *Methylosinus trichosporium* OB3b when expressing its soluble methane monooxygenase enzyme (sMMO). Pseudo-first-order rate constants as high as 2.9 L (mg of TSS)⁻¹ day⁻¹ have been measured with TCE under controlled bench-scale conditions (2). In contrast, mixed cultures generally exhibit much smaller TCE degradation rate constants in the range of 0.005–0.2 L (mg of TSS)⁻¹ day⁻¹ (3–5) with the exception of cultures isolated by Alvarez-Cohen and McCarty (6). *M. trichosporium* OB3b was selected for this work because of the potential for rapid degradation rates.

M. trichosporium OB3b synthesizes two forms of methane monooxygenase (MMO): a particulate enzyme (pMMO) associated with the extensive internal membrane system of these organisms and a soluble enzyme (sMMO) (7). sMMO exhibits much broader substrate specificity and catalytic activity than the particulate form and, consequently, is the active catalyst in the cometabolic transformation of chlorinated solvents. The relative amount of sMMO and pMMO synthesized is dependent upon the amount of copper present in the environment (8, 9). Unfortunately, in the presence of as little as 15 µg/L Cu(II), a concentration similar to that found in many natural waters (10), sMMO synthesis is eliminated in wild-type *M. tri-*

* Corresponding author telephone: 512-471-4996 fax: 512-471-0592; e-mail address: Speitel@mail.utexas.edu.

[†] Department of Civil Engineering.

[‡] Department of Chemical Engineering.

chosporium OB3b. To circumvent this problem, mutant strains of *M. trichosporium* OB3b were developed that exhibited sMMO expression and rapid rates of chlorinated solvent cometabolism in the presence of high levels of copper (up to 800 $\mu\text{g/L}$).

M. trichosporium OB3b attaches very poorly to surfaces (11); therefore, biofilm reactors cannot be used with this organism. The organism also tends to be rather sensitive to environmental conditions; thus, a technology that provides significant control over environmental conditions is most desirable from the viewpoint of establishing and maintaining rapid degradation rates. Furthermore, the technology must address the potential for toxicity problems from other components of the waste matrix, as described above for the third category of contamination.

Hollow fiber membrane reactors (HFMR) were studied in this research as a novel means of meeting the criteria outlined above for successfully treating a broad range of contamination using *M. trichosporium* OB3b. The reactor consists of a large number of tubular membranes (fibers) encased in a cylindrical shell in an analogous manner to a shell and tube heat exchanger. Contaminated water flows through the inside (lumen) of the membranes, and a solution containing the bacteria flows across the outside (shell side) of the membranes. Thus, the bacteria are in suspension and circulate through the HFMR and back to an external reactor where methane and oxygen are supplied for bacterial growth.

The membrane fibers are fabricated from a highly porous hydrophobic material, such as polypropylene. Because the membranes are hydrophobic, water in the shell and lumen will not enter the pore space within the fiber wall. Volatile chemicals, such as chlorinated solvents, can cross the membrane by volatilizing from the lumen solution, diffusing through the pore space vapor, and dissolving in the water on the other side of the membrane. Nonvolatile chemicals, such as heavy metals, cannot pass through the membrane in this fashion. Thus, the membrane provides a barrier between the organisms and the contaminated water, allowing independent control of the microbial environment and no direct contact with the contaminated water being treated. The HFMR system also protects the organisms from copper in the contaminated water, because copper cannot cross the membranes. The copper sensitivity of the wild-type organism is so great, however, that even trace concentrations of copper in nutrient solutions can shut off production of sMMO. Thus, the use of copper-resistant mutant strains, even in HFMR systems, is a practical necessity.

The HFMR system provides the additional advantage of avoiding enzyme competition between the growth substrate (methane) and the chlorinated solvents. Methane is supplied and consumed in an external reactor, while chlorinated solvents are degraded within the HFMR. Thus, the methane and chlorinated solvents are spatially separated and cannot compete for the reactive site on the sMMO, thereby allowing more rapid rates of chlorinated solvent cometabolism.

The primary goal of this research was to demonstrate the technical feasibility of the process. Secondary goals included measurement of mass transfer rates and development of a mathematical model of the process. The model provides a conceptual basis for data analysis and interpretation and, in the future, may serve as a design tool. The research goals were addressed through bench-scale experi-

ments designed to demonstrate the rate and extent of biodegradation. Other abiotic experiments were conducted to measure mass transfer rates. The model was used both as a data fitting tool and in a predictive manner in evaluating the laboratory data.

Materials and Methods

Chemicals. TCE was selected as the model chlorinated solvent for this research because of its widespread occurrence in the environment. ^{14}C -Radiolabeled TCE (Sigma Chemical Co., specific activity 4.1 mCi/mmol, 99% pure) was used to follow the fate of TCE in some mass transfer and biodegradation experiments. [^{14}C]TCE was stored in a 99% methanol/1% ethanol solution at 4 °C. The unlabeled TCE was 99% pure. Pesticide-grade *n*-pentane (Fisher Scientific) was used for TCE extractions. Methane for microbial growth was obtained from compressed gas cylinders containing at least 93% methane or from the local natural gas supply.

Microbial Culture. A mutant strain of *M. trichosporium* OB3b, strain PP358 (ATCC 55314), developed at the University of Texas at Austin, was used in this research (12). Strain PP358 used in this research also had antibiotic resistance. Streptomycin and nalidixic acid were added to culture media as a means of minimizing contamination of cultures by other organisms. The usefulness of antibiotic resistance in practice is unclear. Continuous addition may be economically infeasible, but periodic dosing to maintain dominance of the desired strain of *M. trichosporium* OB3b may be workable.

Thompson's media (13) was used as the nutrient medium for cell suspensions in the HFMR. Streptomycin sulfate, nalidixic acid, and cyclohexamide (to prevent fungal growth) were filter-sterilized and added to the media, each at a concentration of 15 mg/L. Tetrasodium pyrophosphate, a sequestering agent that retards the attachment of bacteria, was also added at a concentration of 1% to protect against biofouling of the membranes.

Analytical Methods. Radioactivity was measured by liquid scintillation counting using a Beckman LS 5000 TD scintillation counter. Quench correction was accomplished using the H-number technique and the instrument's internal cesium-137 source. The scintillation cocktail used was ScintiVerse II (Fisher Scientific).

The biomass concentration was quantified by optical density through measurement of absorbance at 600 nm in a 1-cm cell. A calibration curve was developed to express biomass in milligrams per liter of TSS (14) as a function of absorbance.

A liquid-liquid extraction technique was employed to extract TCE from aqueous samples prior to quantification using gas chromatography. Samples in 25-mL vials were extracted with 2 mL of pentane by agitating the sample headspace-free on a shaker table for 30 min. The pentane was spiked with 1 mg/L chloroform, which served as an internal standard for gas chromatographic analysis. The pentane extract was injected into a DB-624 megabore column (J&W Scientific) connected to an electron capture detector. The same chromatography column was connected to an FID detector for analysis of gas samples.

Hollow Fiber Membrane Reactor. The hollow fiber membrane reactor was a radial, cross-flow Liqui-Cel prototype module manufactured by Hoechst Celanese. A central distribution tube was surrounded by the fiber bundle that was parallel and concentric to the cylindrical shell.

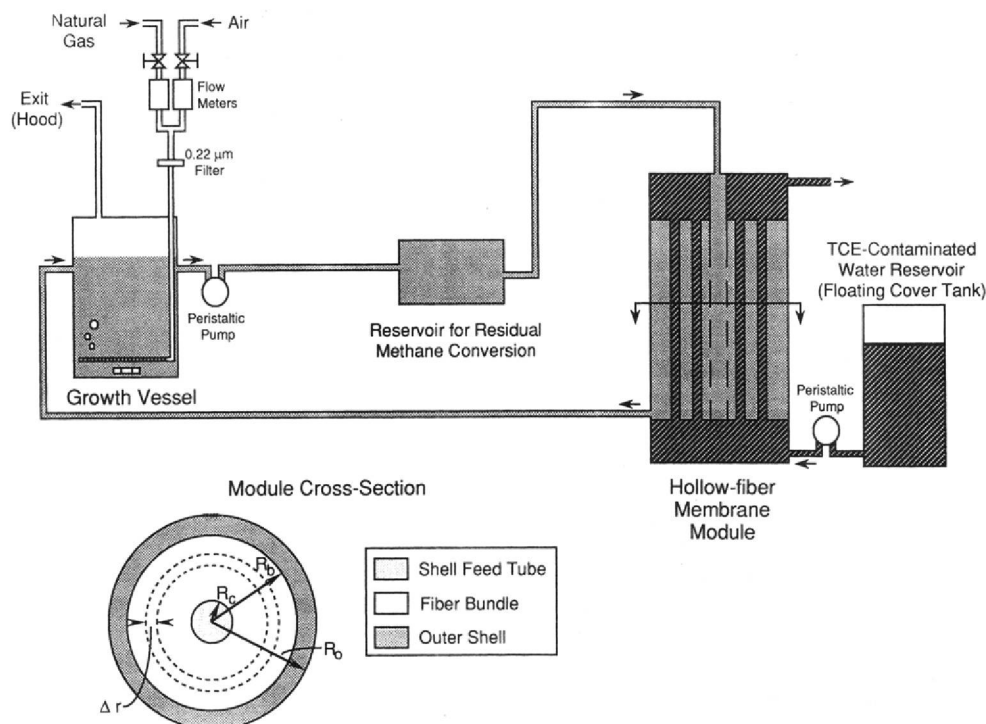


FIGURE 1. Hollow fiber membrane reactor apparatus.

TABLE 1
Hollow Fiber Membrane Module Specifications

parameter	value
no. of fibers	5600
fiber i.d. (μm)	240
effective fiber length (cm)	23.9
surface area (cm^2)	10,091
fiber bundle porosity	0.58
lumen-side volume (mL)	57.8
shell-side volume (mL)	147
module length (cm)	30.3
diameter (cm)	5.1
fiber type	Celgard x-10
fiber material	polypropylene
fiber wall thickness (μm)	30
fiber wall porosity (%)	30
effective pore size (μm)	0.05

The shell-side influent fluid flowed through the central distribution pipe and into the shell through 32 holes drilled in groups of four at eight locations along the pipe's length. The fluid flowed perpendicular to the fibers, up the side wall of the module and through the outlet channel at the top. Table 1 outlines the module dimensions.

Figure 1 presents a process schematic of the entire experimental system. The 20-L cell suspension reservoir (10-L working volume) was seeded with PP358 that had been cultured in smaller vessels. Methane and air were supplied continuously. When a 200 mg of TSS/L culture was obtained in the reservoir, the cell suspension was circulated through a glass holding tank to remove methane, through the shell side of the hollow fiber membrane module, and back to the reservoir using a variable-speed peristaltic pump. TCE-contaminated water was pumped from a 20-L stainless steel floating cover tank through the lumen using a variable-speed peristaltic pump. In this way, metabolism and cometabolism were spatially sequenced to avoid competition of methane and TCE for sMMO. The cell suspension reservoir was operated in a semi-batch mode.

TABLE 2
Experimental Conditions

exp. ^a	influent lumen concn ($\mu\text{g/L}$)	lumen residence time (min)	shell residence time (min)	cell concn (mg of TSS/L)
MT1	172	5.8	8.4	0
MT2	225	13.4	9.1	0
MT3	174	14.1	13.2	0
MT4	194	3.0	5.8	0
MT5	120	10.3	11.8	0
MT6	585	11.6	1.5	0
MT7	709	11.6	2.9	0
MT8	690	11.6	4.9	0
MT9	633	11.6	14.7	0
B1	90	9.4	14.5	200–400
B2	120	5.0	9.3	250–350

^a MT, mass transfer; B, biodegradation.

To maintain the culture in exponential growth phase, 50–75% of the cell suspension was wasted and replenished with nutrient media whenever the cell concentration reached 400 mg TSS/L. The HFMR was operated at ambient temperature with aerobic conditions maintained throughout the system. The experimental conditions for the mass transfer and biodegradation studies are summarized in Table 2.

Hollow Fiber Membrane Biodegradation Experiments. For biodegradation experiments, TCE-contaminated water was fed through the lumen side of the hollow fiber membrane module, and suspended PP358 cell culture was pumped through the shell side. Radiolabeled TCE was used for the first part of both bioreactor experiments. The target radioactivity was approximately 800 dpm/mL in the TCE-contaminated water to be treated, while the unlabeled TCE ranged from 100 to 200 $\mu\text{g/L}$.

Samples for gas chromatographic and radiochemical analyses were taken periodically from the lumen inlet, shell inlet, lumen outlet, and shell outlet using a syringe. Shell-

side samples were injected with 0.2 mL of 6 N HCl to kill bacteria before being sealed headspace-free and refrigerated at 4 °C until extraction and gas chromatographic analysis. Samples of cell suspension were also taken periodically from the reservoir for batch kinetic experiments.

To determine the amount of TCE degraded and $^{14}\text{CO}_2$ and ^{14}C -labeled nonvolatiles formed, each sample was divided into three 7-mL aliquots. One aliquot was mixed with 5 mL of scintillation cocktail and counted to measure total radioactivity. The second aliquot was acidified with 0.1 mL of 6 N HCl, purged with air for 7 min to drive off $^{14}\text{CO}_2$ and $[^{14}\text{C}]\text{TCE}$, and then mixed with scintillation cocktail prior to being counted. The last aliquot was added to 0.2 mL of Carbosorb (an organic base), purged with air for 7 min to drive off $[^{14}\text{C}]\text{TCE}$, mixed with scintillation cocktail, and counted. A background total radioactivity count was taken from a 7-mL sample of nutrient solution. These samples were termed total, acid, base, and background, respectively.

The following equations were used to determine the radioactivity contributed by TCE, CO_2 , and nonvolatile byproducts.

$$\text{TCE} = \text{total} - \text{base} \quad (1)$$

$$\text{CO}_2 = \text{base} - \text{acid} \quad (2)$$

$$\text{byproducts} = \text{acid} - \text{background} \quad (3)$$

Batch Kinetics Experiments. Batch kinetics experiments were carried out on cell suspensions during HFMR biodegradation experiments to quantify TCE degradation rate constants. Each time the rate constant was measured, three 250-mL amber bottles, each with a Mininert Teflon valve and silicone septum, were filled with 50 mL of culture. In addition, one 250-mL bottle was filled with 50 mL of nutrient water to serve as a standard. For some tests, the cell culture was diluted with sterilized nutrient solution to provide a convenient cell concentration. Each bottle was injected with 60 μL of a 1 g/L aqueous TCE stock solution to raise the initial aqueous concentration to 1200 $\mu\text{g}/\text{L}$ after equilibration with headspace vapor, promptly capped, and placed inverted on a shaker table operating at ambient temperature. Between three and five 1-mL headspace samples were collected from each bottle over time and were analyzed by gas chromatography.

A TCE calibration was established by assuming a linear concentration to peak area relationship. The averaged peak areas of the standard were divided into the equilibrium liquid phase concentration to yield the calibration.

The degradation of TCE by PP358 was assumed to follow a pseudo-first-order rate expression, as represented by the following equation for batch reactors:

$$\text{rate} = dC_L/dt = -k_1XC_L \quad (4)$$

where C_L is the liquid phase TCE concentration at time t , X is the biomass concentration, assumed to remain constant over the course of the experiment, and k_1 is the pseudo-first-order degradation rate constant. This equation was modified to account for the partitioning of TCE between the gas and liquid phases by incorporating Henry's constant (0.415 at 25 °C). A mass balance on TCE in the bottle and substitution of $C_G = HC_L$ yielded the following integrated form of the degradation equation:

$$\ln C_L = \frac{-k_1Xt}{1 + H(V_G/V_L)} + \ln C_{L_0} \quad (5)$$

where C_{L_0} is the initial liquid phase cell concentration, V_G is the volume of gas, and V_L is the volume of liquid in the bottle. Linear regression performed on $\ln C$ versus time data generated a slope equal to $-k_1X/[1 + H(V_G/V_L)]$, thereby allowing the determination of k_1 .

Mass Transfer Studies. Separate abiotic experiments were conducted to characterize mass transfer in the HFMR. A solution of unlabeled TCE was pumped through the lumen, while distilled water was pumped through the shell. Samples were taken every few hours from the lumen inlet, lumen outlet, and shell outlet lines using a 30-mL glass Multifit syringe. Each sample was then smoothly injected into a vial, sealed headspace-free using a screw cap with a Teflon-coated silicone septum, and later extracted with pentane prior to gas chromatographic analysis.

Modeling of Radial-Flow Hollow Fiber Membrane Reactor. A mathematical model of the HFMR was developed to provide a conceptual framework for quantifying the relationships among the process variables and to serve as a tool for interpreting experimental data. The model divides the reactor into three sections, as shown in Figure 1. In the center of the reactor is the shell feed tube of radius R_c , which extends along the entire length of the reactor and evenly distributes the shell influent in a radial-flow pattern. It was assumed that no mass transfer or reactions occur in the feed tube; therefore, the chemical concentration along the length of the feed tube is constant and equal to the shell influent concentration.

Outside the shell feed tube is the fiber bundle, where mass transfer between the lumen and the shell occurs. The fiber bundle consists of an annulus of inner radius R_i and outer radius R_b . Shell fluid was assumed to flow across the fiber bundle perpendicular to the fibers in a radial plug-flow pattern. Because an even distribution of the shell influent flow along the length of the reactor was also assumed, the shell-side velocity is independent of axial position. The fiber distribution was assumed to be uniform within the bundle and was characterized by the bundle porosity, ϵ , which is the fraction of the fiber bundle occupied by the shell-side fluid. Plug-flow conditions were also assumed within the lumen.

Outside the fiber bundle is the outer shell, which extends from the fiber bundle periphery (R_b) to the outer wall of the reactor (R_o). The outer shell contains no fibers and collects the shell fluid for discharge from the reactor. Biodegradation occurs in both the fiber bundle and the outer shell.

The model was developed for steady-state conditions. Because the complexity of the model does not permit an analytical solution, it was solved using numerical integration of a large number of CSTR-like differential elements within the reactor. Each differential element is a cylindrical tube of length Δz and wall thickness Δr . A total and a lumen-side mass balance can be written for each differential element. The mass balances can be solved simultaneously to give the outlet lumen and shell concentrations given the inlet concentrations. By sequentially stepping through the differential elements from the influent to the effluent end of the reactor, the shell and lumen effluent concentrations from the reactor can be calculated.

The total balance on a differential element within the fiber bundle is

$$\begin{aligned}
 & \underbrace{\left(C_{s_{i,j-1}} Q_s \frac{\Delta z}{L} + C_{L_{i-1,j}} Q_L \frac{A_j}{A_T} \right)}_{\text{mass in by advection}} - \\
 & \underbrace{\left(C_{s_{i,j}} Q_s \frac{\Delta z}{L} + C_{L_{i,j}} Q_L \frac{A_j}{A_T} \right)}_{\text{mass out by advection}} - \\
 & \underbrace{\frac{1}{2} (C_{s_{i,j-1}} + C_{s_{i,j}})}_{\text{mass consumed by biodegradation}} k_1 X A_j \Delta z \epsilon = 0 \quad (6)
 \end{aligned}$$

where $C_{s_{i,j}}$ is the shell-side concentration in the i th axial and j th radial element, Q_s is the shell total flow rate, $C_{L_{i,j}}$ is the lumen-side concentration in element (i,j) , Q_L is the lumen flow rate, A_j is the radial cross-sectional area of element (i,j) , A_T is the radial cross-sectional area of the fiber bundle, k_1 is the pseudo-first-order degradation rate constant, and X is the biomass concentration. The arithmetic average concentration in each element is used to calculate the biodegradation rate. The total mass balance can be solved for $C_{s_{i,j}}$ to yield

$$\begin{aligned}
 C_{s_{i,j}} = C_{s_{i,j-1}} & \frac{\left(Q_s \frac{\Delta z}{L} - \frac{1}{2} k_1 X A_j \Delta z \epsilon \right)}{\left(Q_s \frac{\Delta z}{L} + \frac{1}{2} k_1 X A_j \Delta z \epsilon \right)} + \\
 & \frac{C_{L_{i-1,j}} - C_{L_{i,j}}}{\left(Q_s \frac{\Delta z}{L} + \frac{1}{2} k_1 X A_j \Delta z \epsilon \right)} \frac{Q_L A_j}{A_T} \quad (7)
 \end{aligned}$$

The lumen-side mass balance for a differential element within the fiber bundle is

$$\begin{aligned}
 & \underbrace{C_{L_{i-1,j}} Q_L \frac{A_j}{A_T}}_{\text{mass in by advection}} - \underbrace{C_{L_{i,j}} Q_L \frac{A_j}{A_T}}_{\text{mass out by advection}} - \\
 & \underbrace{\frac{1}{2} K_L a \left((C_{L_{i-1,j}} + C_{L_{i,j}}) - (C_{s_{i,j-1}} + C_{s_{i,j}}) \right)}_{\text{mass out by mass transfer}} A_j \Delta z = 0 \quad (8)
 \end{aligned}$$

where K_L is the overall mass transfer coefficient, and a is the specific surface area of fibers within the fiber bundle. This mass balance may be solved for the lumen concentration in element (i,j) , using the total mass balance result, to yield

$$\begin{aligned}
 C_{L_{i,j}} & \left(2Q_L + K_L a A_T \Delta z \left(1 + \frac{2Q_L A_j L}{2Q_s \Delta z A_T + k_1 X A_j A_T L \Delta z \epsilon} \right) \right) = \\
 C_{L_{i-1,j}} & \left(2Q_L - K_L a A_T \Delta z \left(1 - \frac{2Q_L A_j L}{2Q_s \Delta z A_T + k_1 X A_j A_T L \Delta z \epsilon} \right) \right) + \\
 & C_{s_{i,j-1}} K_L a A_T \Delta z \left(1 + \frac{2Q_s - k_1 X A_j L \epsilon}{2Q_s + k_1 X A_j L \epsilon} \right) \quad (9)
 \end{aligned}$$

The shell flow from the fiber bundle feeds into the outer shell, which was also modeled as a series of CSTRs. The

outer shell was divided into cylindrical tubes of length Δz and wall thickness $R_o - R_b$. Each outer shell element receives flow from the fiber bundle and the element prior to itself. The concentration exiting the i th element is found from the mass balance

$$\begin{aligned}
 & \underbrace{i Q_s \frac{\Delta z}{L} C_{s_{o,i-1}}}_{\text{axial flow in from prior element}} + \underbrace{Q_s \frac{\Delta z}{L} C_{s_{i,m-1}}}_{\text{radial flow in from fiber bundle}} - \underbrace{(i+1) Q_s \frac{\Delta z}{L} C_{s_{o,i}}}_{\text{exit flow}} - \\
 & \underbrace{k_1 X C_{s_{o,i}} V}_{\text{degradation}} = 0 \quad (10)
 \end{aligned}$$

where V is the volume of an outer shell element, $C_{s_{i,m-1}}$ is the concentration exiting the fiber bundle at the i th axial element, m is the number of radial elements within the fiber bundle, and $C_{s_{o,i}}$ is the chemical concentration in the i th outer shell element. $C_{s_{o,i}}$ can be calculated by rearranging eq 10:

$$C_{s_{o,i}} = \frac{C_{s_{i,m-1}} + i C_{s_{o,i-1}}}{1 + i + \frac{k_1 X V}{Q_s \Delta z / L}} \quad (11)$$

The effluent concentration from the shell is $C_{s_{o,n}}$, where n is the number of axial differential elements in the reactor.

The equations are solved for the outlet shell and lumen concentrations using the boundary conditions $C_{s_{i,1}} = C_{s_{inlet}}$ for elements $(i,0)$ and $C_{L_{1,j}} = C_{L_{inlet}}$ for elements $(0,j)$. Required input data are the inlet concentrations and flow rates, the mass transfer coefficient, the biomass concentration, and the degradation rate constant. The model may be used for mass transfer with biodegradation or for mass transfer alone by setting X or k_1 (biomass concentration or rate constant) equal to 0.

Results and Discussion

Mass Transfer Studies. A prerequisite for the biodegradation of chlorinated solvents is an adequate mass transfer rate from the lumen to the shell. Mass transfer experiments, MT1–MT9, indicated that TCE was effectively transferred from the lumen-side fluid (Table 3). Over the range of influent TCE concentrations (120–709 $\mu\text{g/L}$) and hydraulic residence times (3–14 min) studied, between 78.3% and 99.9% of the TCE was removed from the lumen. Mass balance closure was satisfactory, ranging from 70 to 121%.

Mass transfer was further quantified by fitting the HFMR model to the data to estimate the overall mass transfer coefficient, K_L . Values of K_L were iteratively selected until the sum of the relative percent errors for the predicted and measured lumen and shell effluent concentration was minimized. The estimated values of K_L are reported in Table 3. The sum of the relative percent errors is also shown to give an indication of how well the model fit the data. Over the experimental conditions employed, K_L ranged from 1.8×10^{-5} to 9.5×10^{-5} cm/s. The largest K_L occurred in experiment MT4, which had the shortest lumen residence time (Table 2).

The overall mass transfer coefficient, K_L , is controlled by three mass transfer resistances acting in series. These include the mass transfer resistances across the liquid films on either side of the membrane and the resistance to diffusion across the air space in the fiber pores. The

TABLE 3

Comparison of Measured Concentrations and Estimated Concentrations from the HFMR Model

exp.	lumen effluent concn		shell effluent concn		estimated K_L (10^{-5} cm/s)	mass closure (%)	residual sum of squares	mass transferred (%)
	measured ($\mu\text{g/L}$)	modeled ($\mu\text{g/L}$)	measured ($\mu\text{g/L}$)	modeled ($\mu\text{g/L}$)				
MT1	25.7	25.7	95.7	83.1	5.3	112	13.3	85.1
MT2	11.5	11.9	67.0	56.6	2.6	117	19.3	94.5
MT3	10.7	10.7	74.3	59.8	2.8	121	19.8	93.4
MT4	42.1	42.1	120	115	9.5	103	3.9	78.3
MT5	19.1	19.1	29.4	45.2	2.3	70	53.9	84.1
MT6	0.5	0.5	29.8	29.7	5.5	102.1	2.9	99.9
MT7	2.9	3.0	72.4	69.5	4.7	102.5	6.9	99.6
MT8	19.0	18.4	113	112	3.3	102.0	4.0	97.3
MT9	130	126	267	253	1.8	105.1	8.1	80.5

relationship between K_L and the three resistances is given as

$$\frac{1}{K_L d_o} = \frac{1}{k_s d_o} + \frac{1}{k_m H d_m} + \frac{1}{k_L d_i} \quad (12)$$

overall mass transfer resistance
shell-side film resistance
membrane resistance
lumen-side film resistance

where d_o is the fiber outside diameter (OD), k_s is the mass transfer coefficient for a liquid film on the outside of a radially swept fiber, k_m is the mass transfer coefficient for diffusion through the fiber, H is Henry's constant, d_m is the log mean diameter of the fiber wall, k_L is the mass transfer coefficient for an axially swept liquid film inside a hollow fiber, and d_i is the fiber inside diameter (i.d.). This representation of K_L with d_o was adapted from Seibert *et al.* (15) as a minor correction to normalize the surface area at each radial position in the fiber to the outer surface area of the fiber.

The dependence of each resistance on hydrodynamic conditions has been characterized in the literature. The shell-side mass transfer coefficient was characterized by Cote *et al.* (16) as

$$k_s = 0.61 d_o^{-0.637} V_r^{0.363} \left(\frac{\rho}{\mu}\right)^{0.023} D^{0.67} \quad (13)$$

where V_r is the radial velocity, and D is the diffusion coefficient of the chlorinated solvent in water. Because V_r is not constant with radial position, k_s , and therefore K_L , it is not constant within the reactor. Instead, K_L is a weak function of radial position, varying approximately 4% across the bundle. Where we report K_L derived from this correlation, the value is reported for the geometric mean radius of the fiber bundle.

The membrane mass transfer coefficient is modeled as diffusion through stagnant air (17):

$$k_m = \frac{\epsilon_m D_{\text{air}}}{\delta} \quad (14)$$

where k_m is the mass transfer coefficient for diffusion through the fiber, ϵ_m is the porosity of the fibers (fraction filled with air), δ is the wall thickness of the fiber, and D_{air} is the diffusion coefficient of the chlorinated solvent in air.

The lumen-side mass transfer coefficient was modeled as (18)

$$k_L = 1.86 \left(\frac{V_z D^2}{L d_i}\right)^{1/3} \quad (15)$$

TABLE 4

Summary of Mass Transfer Experiments

exp.	shell Re	lumen Pe	mass transfer resistances ^a (10^3 s/cm)			
			shell film ^b	lumen film ^c	overall ^{d,e} (correlation)	overall ^f (best fit)
MT1	0.0066	0.183	3.40	3.28	6.68	18.9
MT2	0.0060	0.079	3.50	4.35	7.85	38.5
MT3	0.0042	0.075	4.00	4.42	8.42	35.7
MT4	0.0095	0.354	2.97	2.64	5.61	10.5
MT5	0.0047	0.103	3.85	3.98	7.83	43.5
MT6	0.0370	0.092	1.82	4.14	5.96	18.2
MT7	0.0190	0.092	2.31	4.14	6.45	21.3
MT8	0.0110	0.092	2.80	4.14	6.94	30.3
MT9	0.0037	0.092	4.17	4.14	8.31	55.6

^a Reported for the geometric mean radius, because resistances depend slightly on radial position. ^b $1/k_s$ (eq 13). ^c $d_o/(k_L d_i)$ (eq 15). ^d Fiber resistance is $d_o/(k_m d_m H)$ (eq 14); value is constant at 0.354 s/cm. ^e $1/K_L$.

where k_L is the mass transfer coefficient for an axially swept liquid film inside a hollow fiber, L is the fiber length available for mass transfer, V_z is the fluid velocity in the lumen, D is the diffusion coefficient of the chlorinated solvent in water, and d_i is the fiber inner diameter.

The individual mass transport resistances and the overall mass transport resistance as calculated from the literature correlations are tabulated for each experiment in Table 4. For comparison purposes, the overall mass transport resistance estimated from the best fit of the model is also listed. The calculated lumen and shell resistances are similar in magnitude. Consequently, the flow rates (or hydraulic residence times) in both the shell and lumen strongly affect the overall mass transfer coefficient. In contrast, the calculated membrane resistance is negligible, being less than 0.005% of the overall mass transport resistance.

The literature correlations generally overestimate the overall mass transfer coefficients (and underestimate the overall mass transfer resistance) by a factor of 3–5, in comparison to the values determined from fitting the model to the mass transfer data. Although the K_L values were different, the literature correlations showed the same general trend as the values determined by fitting the model to the data. The source of the disagreement between the literature correlations and the best fit of the model to the data is unclear. One possibility is the difference in the shell Reynolds numbers and lumen Peclet numbers in the experiments versus those used to develop the correlations. In this work, the Reynolds and Peclet numbers were 2–3 orders of magnitude less than those used to develop the

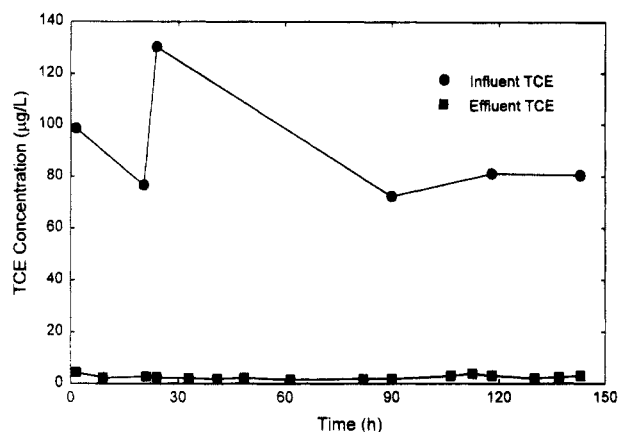


FIGURE 2. Lumen influent and effluent TCE concentrations in experiment B1.

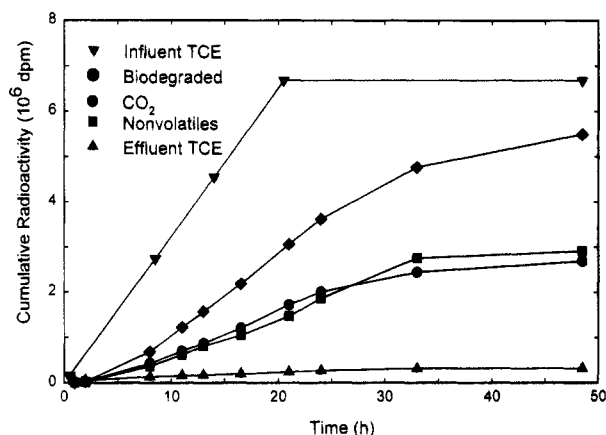


FIGURE 3. Cumulative radioactivity during experiment B1.

correlations. Thus, a considerable extrapolation of the correlations was required. Another possibility is that the actual flow pattern in the reactor may depart from the ideal flow conditions assumed in the modeling. Departures from ideal flow would probably decrease the mass transfer rate, leading to smaller estimated values of K_L when the model is fitted to the data. Further mass transfer studies and tracer tests of reactor hydraulics would be needed to resolve the disagreement.

Biodegradation Experiments. Figure 2 shows the lumen TCE concentrations during experiment B1. The influent TCE concentration ranged from 70 to 130 $\mu\text{g/L}$, with a mean of 90 $\mu\text{g/L}$. Virtually all the influent TCE was removed from the lumen as indicated by the very low lumen effluent concentrations, many of which were near the analytical detection limit. Greater than 90% of the TCE was removed from the lumen at the 9-min lumen and 14-min shell residence times employed in this experiment.

To determine whether TCE removed from the lumen was biodegraded in the shell, the lumen influent was spiked with ^{14}C TCE, and radiochemical analyses were carried out. The radiochemical analyses focused on the membrane reactor only and did not examine biodegradation and volatilization of ^{14}C in the external growth reactor. The performance of the membrane reactor was isolated from that of the rest of the system by measuring influent and effluent radioactivity in both the shell and lumen. Figure 3 presents cumulative radioactivity data for the first 49 h of experiment B1. The influent and effluent TCE data are the cumulative ^{14}C TCE entering and leaving the reactor through the lumen. ^{14}C TCE that is biodegraded by PP358

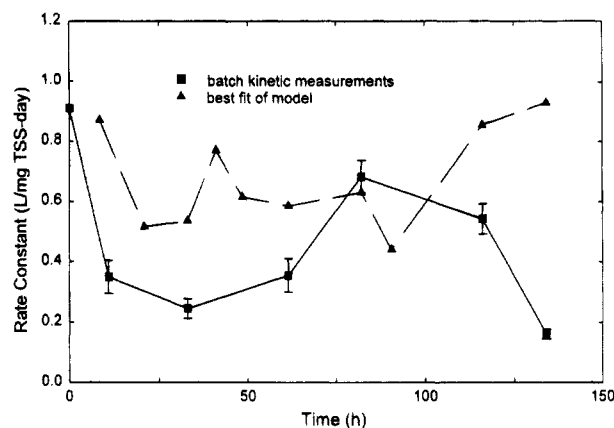


FIGURE 4. Pseudo-first-order rate constants during experiment B1.

is predominantly degraded to $^{14}\text{CO}_2$ and ^{14}C -labeled nonvolatiles (both soluble and particulate). Therefore, the amount degraded is represented by the sum of the CO_2 and nonvolatile radioactivity. Virtually all of the biodegradation products (i.e., $^{14}\text{CO}_2$ and ^{14}C -labeled nonvolatiles) were detected in the shell effluent, indicating that very little back-diffusion of biodegradation products across the membrane occurred. Over 90% of the residual ^{14}C TCE and $^{14}\text{CO}_2$ in the shell effluent was subsequently lost from the system in the external growth reactor, presumably through a combination of biodegradation and volatilization. Most of the ^{14}C -labeled nonvolatiles however remained in the system, indicating that these materials were resistant to further biodegradation.

The lumen influent received ^{14}C TCE for the first 22 h only, but production of $^{14}\text{CO}_2$ and ^{14}C -labeled nonvolatiles continued after ^{14}C TCE addition had ceased. Biodegradation continued because a portion of the ^{14}C TCE added to the influent had adsorbed during the first 22 h and subsequently desorbed after ^{14}C TCE addition had stopped. The biomass in the shell continued to degrade the desorbed ^{14}C TCE as evidenced by the presence of $^{14}\text{CO}_2$ and ^{14}C -labeled nonvolatiles in the effluent after 22 h of operation. Adsorption of TCE on the polypropylene membranes at the start of experiments was regularly observed with both radiolabeled and unlabeled TCE.

To calculate the percentage of transferred TCE biodegraded in the shell, the net CO_2 and nonvolatile radioactivity (i.e., reactor effluent minus influent) were summed and divided by the radioactivity removed from the lumen. The percent biodegraded within the shell was 88%, with 42% attributed to CO_2 production and 46% to nonvolatiles. A mass balance across the reactor showed excellent closure, with 96% of the influent radioactivity recovered in the effluent. Thus, the radiochemical data clearly demonstrated that PP358 was effective in biodegrading TCE in this bioreactor configuration.

The radiochemical data confirmed the biodegradation of TCE, but the rate of degradation is also important in engineered systems. The rate affects the required organism concentration and reactor volume. Also, rate data can effectively track the cometabolic activity of the organisms. To determine the rate of TCE biodegradation, rate constants for samples periodically collected from the cell suspension reservoir were measured using the batch headspace technique. Figure 4 presents the pseudo-first-order rate constants and their 95% confidence limits for experiment B1. The value of the rate constant varied from 0.16 to 0.9

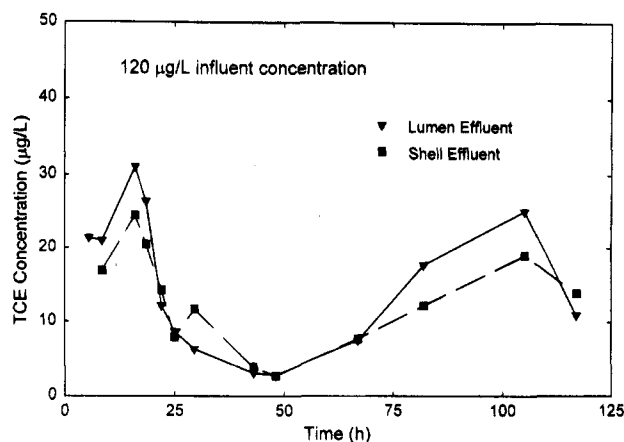


FIGURE 5. Effluent TCE concentration for experiment B2.

L (mg of TSS)⁻¹ day⁻¹ during the experiment. This variation may result from the inherently unsteady state nature of semi-batch operation; more stability in the rate constant should be possible with continuous-flow operation of the cell suspension reservoir. The final decline in the rate constant was due to increasing populations of organisms other than PP358, as evidenced by both a color change and flocculation of the cell suspension.

The range of biodegradation rate constants is comparable to those obtained in batch studies under ideal conditions and is considerably larger than those obtained with other bioreactor configurations. Rate constants have been in the range of 0.5–3 L (mg of TSS)⁻¹ day⁻¹ for batch biodegradation studies using OB3b (2, 9, 12, 13). For pure OB3b cultures seeded on packed columns and operated in cyclic feed and degradation modes, maximum pseudo-first-order rate constants were in the range of 0.01–0.08 L (mg of cells)⁻¹ day⁻¹ (11). These rate constants, however, could be maintained for only short periods of time and usually declined to much lower values in less than 1 day. Thus, at least 1 order of magnitude higher rate constants were sustained in the HFMR for a much longer period of time. In the context of practical applications, however, the high rate constants probably would have to be sustained for even longer periods, perhaps on the order of several weeks or months.

In experiment B1, the shell and lumen effluent concentrations were near the detection limits of the gas chromatograph. To increase the effluent concentrations, lumen and shell flow rates were increased in experiment B2. Figure 5 presents the TCE concentration in the lumen and shell effluents for experiment B2. Of the 120 µg/L TCE entering the reactor in the influent, between 3 and 32 µg/L exited in the lumen effluent. This corresponded to between 73 and 98% transferred to the shell. The variability was likely due to changing microbial activity over the course of the experiment. Figure 6 shows how the rate constant measured in batch assays varied over time during experiment B2. The measured rate constant varied between 0.41 and 0.58 L (mg of TSS)⁻¹ day⁻¹ but again declined rapidly near the end of experiment B2 as a result of contamination by other organisms. The biodegradation rate constants in experiment B2 were comparable to those of experiment B1, and the relatively low lumen and shell effluent concentrations indicate that successful operation can be achieved at shorter shell and lumen residence times than used in experiment B1. The presence of measurable TCE concentrations in the shell and lumen effluents, however,

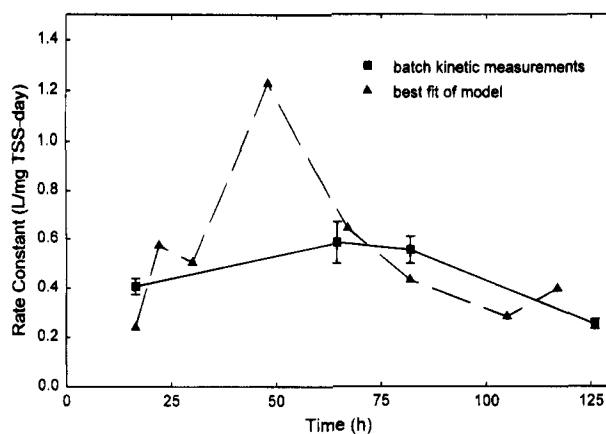


FIGURE 6. Pseudo-first-order rate constants during experiment B2.

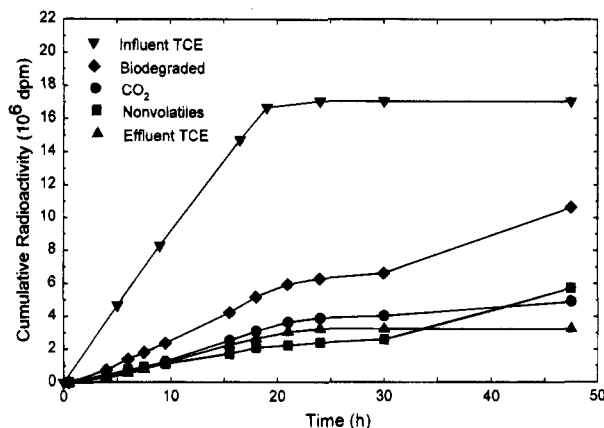


FIGURE 7. Cumulative radioactivity during experiment B2.

suggests that a larger biomass concentration would have been desirable to promote greater biodegradation in the shell. The mass transfer rate from the lumen would also have increased because a larger concentration gradient would be established across the membranes.

As with experiment B1, [¹⁴C]TCE was added to the lumen influent for the first 19.5 h of operation to confirm the biodegradation of TCE. A cumulative radioactivity plot for experiment B2 is presented in Figure 7. Reactor performance was similar to that in experiment B1, except that more TCE left in the lumen effluent because of the shorter hydraulic residence time in the lumen. Of the [¹⁴C]TCE transferred from the lumen to the shell, 77% was biodegraded within the shell, with 36% attributed to CO₂ production and 41% to nonvolatiles. The mass balance closure was 101%. The slightly smaller percent biodegradation relative to experiment B1 probably resulted from the shorter hydraulic residence time in the shell. The relative proportions of the degradation products were approximately the same in each experiment. For comparative purposes, the radiochemical results for experiments B1 and B2 are summarized in Table 5.

Biodegradation Modeling. To assist in interpreting experimental results, the model was fitted to the experimental data for each sampling time by adjusting both the biodegradation rate constant and the overall mass transfer coefficient until the measured and simulated lumen and shell effluent concentrations exactly matched. The best-fit values of k_1 for experiment B1 are shown in Figure 4. The average best-fit value of K_L was 8.5×10^{-5} cm/s with a 95% confidence interval of $\pm 0.84 \times 10^{-5}$ cm/s. It is interesting to compare the K_L values from the biodegradation experi-

TABLE 5

Summary of Radiochemical Data in Biodegradation Experiments

exp.	lumen influent concn ($\mu\text{g/L}$)	lumen residence time (min)	shell residence time (min)	% removed from lumen	% biodegraded in shell	% converted to ^{14}C in shell	% converted to ^{14}C -labeled nonvolatiles in shell
B1	90	9.4	14.5	95.3	88	42	46
B2	120	5.0	9.3	81.0	77	36	41

ments to those developed in the mass transfer studies. Experiment B1 had similar lumen and shell residence times to mass transfer experiments MT5 and MT9 (Table 2); therefore, a K_L value of approximately 2×10^{-5} cm/s would be expected in experiment B1 based on the mass transfer studies. In contrast, the best-fit value was over four times greater, which implies that mass transfer was somehow enhanced in the presence of microbial activity. One possible mechanism for this enhancement is biodegradation within the shell-side liquid film, which would accelerate the mass transfer rate. As shown in Figure 4, the best-fit biodegradation rate constants were generally larger than those estimated from batch kinetics tests on samples taken from the external growth reactor. This difference may be an artifact of the measurement technique. In the batch experiments, the organisms must be held in the absence of growth substrate for several hours, which may adversely affect sMMO and energy levels, leading to biased estimates of the k_1 . In contrast, the organisms were deprived of growth substrate for a much shorter period in the HFMR system, which may result in greater sMMO activity.

An identical analysis was performed on experiment B2. The best-fit values of k_1 for experiment B2 are shown in Figure 6. The best-fit biodegradation rate constants again tended to be larger than those estimated from batch kinetics tests on samples taken from the external growth reactor. The average best-fit value of K_L was 9.9×10^{-5} cm/s with a 95% confidence interval of $\pm 4.7 \times 10^{-5}$ cm/s. The corresponding K_L value from the mass transfer experiments (experiment MT1) was 5.3×10^{-5} cm/s. Again, the best-fit value of K_L was greater than expected based on the results of the mass transfer studies. Thus, the results from experiment B2 are consistent with those of experiment B1 and support the conclusions drawn from experiment B1. The modeling suggests two areas for further investigation: the possibility of enhanced mass transfer rates when organisms are present and the refinement of batch testing techniques so that k_1 is not underestimated. Further work in these areas may improve the accuracy of the model when it is used in a predictive (versus data fitting) fashion in reactor design.

Acknowledgments

The authors gratefully acknowledge support from the Gulf Coast Hazardous Substance Research Center, the Environmental Solutions Program at the University of Texas at Austin, and the Texas Advanced Technology Research Program. We are also grateful to Hoechst Celanese for providing the membrane modules and for the advice provided by Dr. Patricia Phelps.

Nomenclature

a	specific surface area of fibers in the fiber bundle, cm^2/cm^3
A_j	radial cross-sectional area of element (i, j), cm^2
A_T	radial cross-sectional area of fiber bundle, cm^2

C_L	lumen-side TCE concentration, $\mu\text{g/L}$
C_s	shell-side TCE concentration, $\mu\text{g/L}$
C_{so}	outer shell concentration, $\mu\text{g/L}$
d_m	log mean diameter of the fiber wall, cm
d_i	fiber inner diameter, cm
d_o	fiber outer diameter, cm
d_s	inside diameter of shell, cm
D	diffusion coefficient of TCE in water, cm^2/s
D_{air}	diffusion coefficient of TCE in air, cm^2/s
ϵ	bundle porosity
ϵ_m	membrane porosity
H	Henry's law constant
(i, j)	numbering of differential element (axial, radial)
K_L	overall mass transfer coefficient, cm/s
k_L	lumen-side mass transfer coefficient, cm/s
k_s	shell-side mass transfer coefficient, cm/s
k_m	mass transfer coefficient for diffusion through fiber membrane, cm/s
k_1	pseudo-first-order degradation rate constant, $(\text{mg of TSS})^{-1} \text{day}^{-1}$
L	module effective length (fiber length), cm
n_f	number of fibers
Pe	Peclet number
Q_L	lumen flow rate, mL/s
Q_s	shell flow rate, mL/s
Re	Reynolds number
Δr	radial thickness of CSTR-like differential element, cm
R_b	effective fiber bundle outer radius, cm
R_c	center tube outer radius, cm
R_o	outer radius (inner side) of HFMR, cm
V	element volume, cm^3
V_r	radial velocity, cm/s
V_z	fluid velocity in lumen, cm/s
Δz	length of CSTR-like differential element, cm
δ	wall thickness of fiber, cm
ρ	density of water, g/mL
μ	viscosity of water, $\text{g cm}^{-1} \text{s}^{-1}$

Literature Cited

- (1) *Survey of Materials-Handling Technologies Used at Hazardous Waste Sites*; U.S. Environmental Protection Agency, Office of Research and Development, U. S. Government Printing Office: Washington, DC, 1991; EPA/540/2-91/010.
- (2) Oldenhuis, R.; Oedzes, J. Y.; Van der Waarde, J. J.; Janssen, D. B. *Appl. Environ. Microbiol.* **1991**, *57*, 7.
- (3) Strand, S. E.; Bjelland, M. D.; Stensel, H. D. *Res. J. Water Pollut. Control Fed.* **1990**, *62*, 124.
- (4) Leeson, A.; Bouwer *Proceedings, Annual Conference of the American Water Works Association*, Los Angeles, CA; American Water Works Association: Denver, CO, 1989.

- (5) Fogel, M. M.; Taddeo, A. R.; Fogel, S. *Appl. Environ. Microbiol.* **1986**, *51*, 720.
- (6) Alvarez-Cohen, L.; McCarty, P. L. *Appl. Environ. Microbiol.* **1991**, *57*, 228.
- (7) Anthony, C. *Adv. Microb. Physiol.* **1986**, *27*, 113.
- (8) Stanley, S. H.; Prior, S. D.; Leak, D. J.; Dalton, H. *Biotechnol. Lett.* **1983**, *5*, 487.
- (9) Tsien, H.; Brusseau, G. A.; Hanson, R. S.; Wackett, L. P. *Appl. Environ. Microbiol.* **1989**, *55*, 3155.
- (10) Forstner, U.; Wittman, G. T. W. *Metal pollution in the aquatic environment*; Springer-Verlag: New York, 1979; p 356.
- (11) Speitel, G. E., Jr.; Segar, R. L., Jr. *Water Sci. Technol.* **1995**, *31*, 215.
- (12) Phelps, P. A.; Agarwal, S. K.; Speitel, G. E., Jr.; Georgiou, G. *Appl. Environ. Microbiol.* **1992**, *58*, 3701.
- (13) Speitel, G. E., Jr.; Thompson, R. C.; Weissman, D. *Water Res.* **1993**, *27* (1), 15.
- (14) *Standard Methods for the Examination of Water and Wastewater*, 17th ed.; Clesceri, L. S., Greenburg, A. E., Trussel, R. R., Eds.; American Public Health Association: Washington, DC, 1989.
- (15) Seibert, A. F.; Py, X.; Mshewa, M.; Fair, J. R. *Sep. Sci. Technol.* **1993**, *28* (1-3), 343.
- (16) Cote, P.; Bersillon, J. L.; Huyard, A. *J. Membr. Sci.* **1989**, *47* (1-2), 91.
- (17) Zhang, Q.; Cussler, E. L. *J. Membr. Sci.* **1985**, *23*, 321.
- (18) Yang, M.-C.; Cussler, E. L. *AIChE J.* **1986**, *32* (11), 1910-1916.

Received for review February 14, 1995. Revised manuscript received May 24, 1995. Accepted June 8, 1995.*

ES950094Q

* Abstract published in *Advance ACS Abstracts*, August 1, 1995.